



20

21 **ABSTRACT**

22

23 We hypothesise that there is an overestimation of Global Mean Sea Level (GMSL) variability
24 from GMSL empirical orthogonal function (EOF) reconstructions due to differences between
25 the tide gauge observations and their corresponding altimetry data. We show that these
26 differences are correlated well with local winds along coastlines, suggesting that observations
27 from tide gauges at the coast and satellite altimetry near the coast could partially be explained
28 by the wind forcing. Correcting these differences through a mainly wind-driven regression
29 model prior to the EOF reconstruction, reduces the standard deviation (SD) of the reconstructed
30 GMSL variability by 26% and significantly increases the correlation to 0.46 with respect to the
31 observed averaged GMSL calculated from altimetry grid points (1994 to 2020). The model was
32 used to extrapolate these differences prior to 1993 and a corrected GMSL reconstruction is
33 presented.

34

35 **KEYWORDS**

36

37 Sea Level, GMSL, EOF Reconstruction, Variability, Wind

38

39 **1. Introduction**

40

41 Global Mean Sea level (GMSL) changes are primarily the result of ocean heat uptake and ice
42 mass loss from glaciers and ice sheets. Consequently, measuring GMSL has become an
43 important factor to assess the health of the world's climate, by providing observational
44 evidence of climate system response to the warming of the planet due to increased greenhouse



45 gases (IPCC 2021). The GMSL variability is a fundamental part in understanding the sea level
46 budget, for example, the contributions of ice mass loss from glaciers and warming of the ocean
47 for individual years/decades. Satellite observations that include GRACE (ocean mass) and
48 altimetry have provided a major tool in understanding mechanisms such as ocean warming and
49 land ice melt by studying the sea level budget (WCRP Global Sea Level Budget Group, 2018).
50 However, GMSL has only been observed directly through satellite altimetry since late 1992.
51 Prior to this, measurements of sea level come primarily from tide gauges and, thus, are
52 restricted to coastal locations. Therefore, there is a need to improve the GMSL variability
53 estimates prior 1993.

54

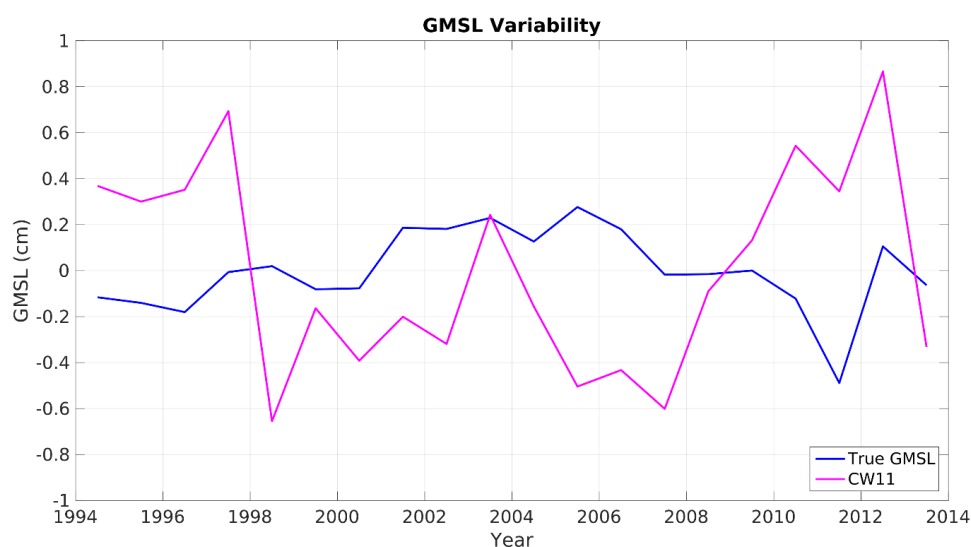
55 One of the most widely used methods to produce global sea level reconstructions for the pre-
56 altimetry era is the reduced space optimal interpolation (RSOI) technique (Kaplan et al. 1997,
57 and 2000). This technique involves inferring empirical orthogonal functions (EOFs) from
58 altimetry data and then fitting a subset of those to tide gauge records to estimate the temporal
59 amplitude associated with each EOF. A spatially uniform EOF (often called EOF0) is typically
60 added to the subset of original EOFs, as first proposed by Church et al. (2004), because
61 otherwise the long-term trends are not adequately reconstructed. We refer to such
62 reconstructions as EOF reconstructions. Other examples of these reconstructions include
63 Church and White (2006), Church and White (2011); Mu, et al. (2018); Ray and Douglas
64 (2011); and Strassburg, et al. (2014).

65

66 Past studies have shown that, while including an EOF0 significantly improves the estimation
67 of the underlying long-term trend in GMSL, it comes at the cost of losing the ability to
68 reconstruct the interannual to decadal variability (Calafat and Gomis, 2009; Calafat et al.,
69 2014). To illustrate this issue, we show a comparison between detrended de-seasoned ‘true’



70 GMSL from the gridded global CMEMS altimetry product (a simple global average per time
71 step) and the GMSL EOF reconstruction from Church and White (2011; hereinafter CW11)
72 updated to include data up to 2013 (Fig. 1). The two time series show little resemblance with
73 a correlation of -0.34. Furthermore, the reconstructed GMSL overestimates the variability by a
74 factor of more than two (SDs of 0.45 cm and 0.18 cm for the reconstruction and the true GMSL
75 observations, respectively). An accurate representation of the variability in GMSL is important,
76 not only because it reveals useful information on the global hydrological cycle (Llovel et al.,
77 2011), but also because it influences the estimation of underlying long-term trends and
78 accelerations in GMSL. Hamlington et al. (2020) examined the steric and barystatic
79 contributions to interannual to decadal variability in GMSL back to 1982 and found that both
80 are highly correlated with the ENSO variations and contribute equally to observed GMSL
81 variability. Sea level variability is becoming increasingly significant as it contributes to coastal
82 flooding and erosion (Widlansky, et al. 2020).



83

84 **Figure 1** The true GMSL variability from CMEMS altimetry and an updated dataset CW11

85 (Church and White, 2011) for the period 1994 to 2013.



86 Noting the issues that arise when including an EOF0, some studies have developed hybrid sea-
87 level reconstructions where the variability is derived from EOF reconstructions without the
88 EOF0 whereas the trends are estimated using other methods such as Bayesian fingerprinting
89 (Dangendorf et al., 2019; Dangendorf et al., 2021; Dangendorf et al., 2023). Such hybrid
90 reconstructions appear to produce good estimates of both the variability and the underlying
91 trends, but they also come with challenges compared to using a unified statistical method, such
92 as potential distortions in the reconstructed time series if the two components do not integrate
93 well and also increased complexity. In this study, we explore ways of improving the estimation
94 of the GMSL variability in EOF reconstructions that include the EOF0.

95

96 While the sparseness of the tide gauge data in time and space is likely to affect the skill of EOF
97 reconstructions (Calafat and Gomis, 2009; Calafat et al., 2014; Christiansen et al., 2010;
98 Natarov et al., 2017), it alone does not explain why EOF reconstructions with an EOF0 fail to
99 capture the GMSL variability. We know this because reconstructions that do not include an
100 EOF0 are able to capture the variability in GMSL with relatively good accuracy. Indeed,
101 Calafat et al. (2014) showed, based on a series of numerical experiments, that the low skill of
102 EOF reconstructions (with an EOF0) to capture the short-term GMSL variability is largely due
103 to differences between tide gauges and the corresponding altimetry point. Such differences
104 arise mainly due to the degradation of the satellite altimetry data within ~10-20 km of the coast
105 (Cipollini et al., 2017). Calafat et al. (2014) showed that if the tide gauges in an EOF
106 reconstruction are replaced by the corresponding altimetry points (i.e., altimetry coastal points
107 are used as virtual tide gauges), effectively removing any differences between tide gauges and
108 altimetry, the variability in GMSL is well captured even when including an EOF0. This
109 demonstrates the crucial role that differences between tide gauges and altimetry play in the
110 reduced skill of EOF reconstructions.



111

112 With a view of improving the skill of EOF reconstructions that include an EOF0, we investigate
113 the nature of the differences between the tide gauge and altimetry signals (hereafter referred to
114 as Signal Differences). We show that such differences have a coherent spatial structure along
115 the coast, suggesting a geophysical origin as opposed to being caused by random errors.
116 Further, we show that the Signal Differences are significantly correlated with wind variability.
117 This allows us to model the Signal Differences at each tide gauge site through linear regression
118 for the whole period of the reconstruction (using wind data from reanalyses) and subtract them
119 from the tide gauge data prior to using them in an EOF reconstruction. We show that this leads
120 to an improved reconstruction of the GMSL variability (1941 to 2020).

121 **2. Data and Methods**

122

123 *2.1 Tide Gauge data*

124

125 Monthly mean values of sea level from tide gauge records were obtained from the Permanent
126 Service for Mean Sea Level (PSMSL) archive (Holgate et al., 2013). For consistency, we use
127 the same tide gauge stations as those used in the CW11 reconstruction. Note that these include
128 both Revised Local Reference (RLR) data and Metric data. In particular, a total of 602 tide
129 gauges were used in the reconstruction, consisting of 491 RLR records (81.6%) and 111 Metric
130 records (18.4%) starting from 1901.

131

132 The monthly tide gauge data had the PSMSL quality control flags applied before the annual
133 and semi-annual cycles were removed by harmonic analysis over the entire period covered for
134 each tide gauge record. The monthly tide gauge records were then corrected for Glacial
135 Isostatic Adjustment (GIA) using the ICE5Gv1.3 (VM2_L90_2012) model for the relative sea



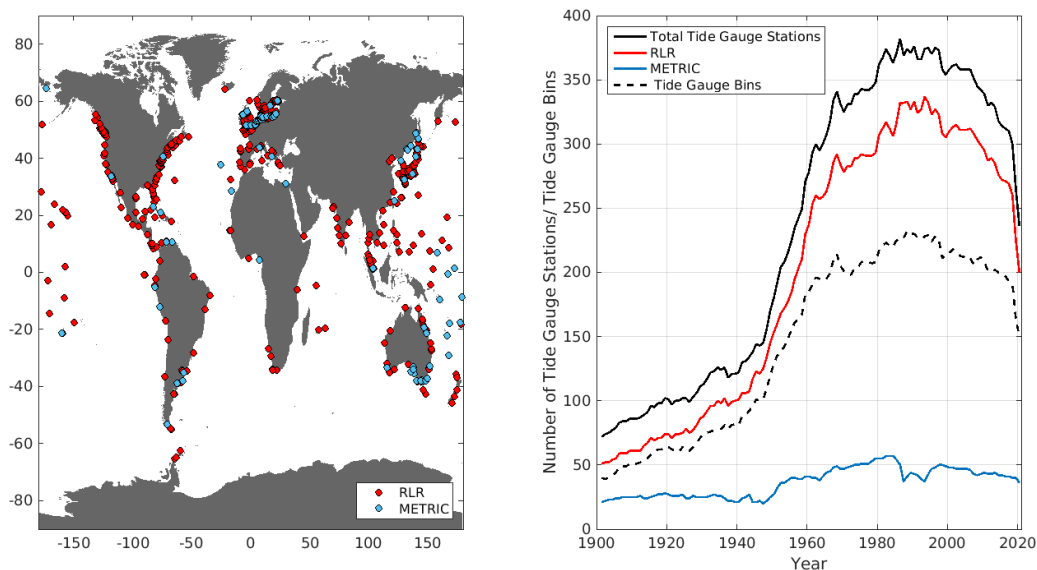
136 level (Peltier, 2004). These GIA values are available on the PSMSL website. The tide gauge
137 data were also adjusted for atmospheric pressure changes using the inverse barometer (IB)
138 approximation. The atmospheric pressure data were obtained from the 20th Century reanalysis
139 (Compo et al., 2011) for the period 1901-1947 and from the NCEP/NCAR reanalysis (Kalnay
140 et al., 1996) for the period 1948-2020. To merge the two atmospheric pressure datasets and
141 ensure their consistency, we forced the two products to have the same time-mean pressure over
142 their overlapping period (1948-2012). For further quality control, each tide gauge record was
143 visually inspected. If any datum shifts were suspected within the time series, then the record in
144 question was compared with records from nearby stations to confirm validity. If a shift was
145 detected and confirmed, then the tide gauge record was split into segments and treated
146 separately. A second pass for each monthly tide gauge record was carried out, removing any
147 observations that were five SDs from the mean. This was to ensure that outliers were removed.
148 A total of 36 values were removed from the entire dataset during this process.

149

150 The monthly tide gauge records were then averaged into yearly values, where a requirement of
151 having at least seven months of observations within the same year was imposed. Following
152 CW11, each record was then differentiated in time using first differences between adjacent
153 years (hereafter denoted by successive differences), effectively placing all the tide gauge
154 records on the same vertical reference frame. We note that the reconstruction method works
155 with successive differences rather than sea level observations; this is to accommodate the fact
156 that tide gauge observations are using different datums. Any yearly successive differences
157 greater than 0.25 m were removed. This value was chosen to ensure that no yearly value
158 accidentally straddled a datum shift of monthly values within the same year. A total of seven
159 yearly observations were removed from the entire data set during this procedure. Following
160 CW11, the quality-controlled tide gauge stations are spatially averaged (combined) into $1^{\circ} \times 1^{\circ}$



161 grouped tide gauge bins for a total of 285 tide gauge bins. The composite tide gauge time series
162 are then ready for the EOF reconstruction. The spatial and temporal distribution of the PSMSL
163 tide gauge stations and the composite dataset using tide gauge bins are displayed in Fig. 2.



164 **Figure 2** The spatial and temporal distribution of the number of tide gauges used in this study
165 (1901–2020). The dashed black line represents the temporal distribution of the tide
166 gauge bins containing composite tide gauge observations for the EOF GMSL
167 reconstruction.

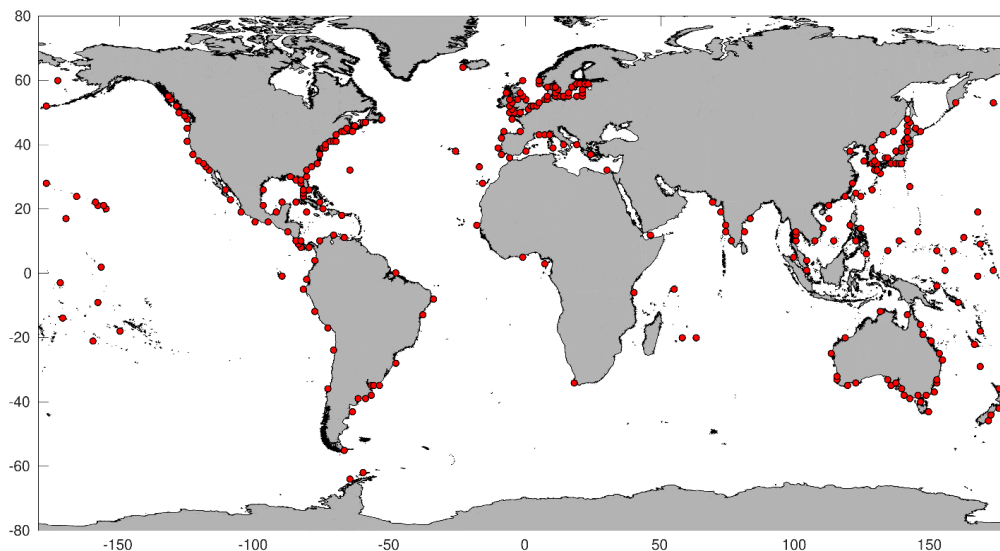
168 2.2 Altimetry dataset

169

170 In this study, we use a multi-mission gridded ($\frac{1}{4}^\circ$ resolution) weekly sea surface height product
171 (SEALEVEL_GLO_PHY_L4_MY_008_047) from the Copernicus Marine Environment
172 Monitoring Service (CMEMS; available at <http://marine.copernicus.eu/>) spanning the period
173 1993 to 2020. The altimetry data had the annual and semi-annual cycles removed using
174 harmonic analysis and the Peltier’s GIA correction (Peltier, 2004) applied
175 (drad250.1grid.ICE5Gv1.3_VM2_L90_2012 dataset). They also had all the standard
176 geophysical corrections applied, including the IB correction.



177 The weekly CMEMS altimetry dataset was converted to yearly values at each $\frac{1}{4}^\circ$ grid cell. The
178 individual tide gauge stations within each tide gauge bin were linked to the closest valid
179 altimetry grid point within a search radius of 50 km. These altimetry points were then spatially
180 averaged if there were more than one in the same bin, producing a subset of the original
181 CMEMS dataset (hereafter referred as the altimetry CMEMS dataset), similar to the CW11 tide
182 gauge binned locations (Fig. 3). All tide gauge stations within the tide gauge bin had a
183 corresponding altimetry timeseries even if they shared the same altimetry pixel location. If this
184 occurred, then they were treated as separate altimetry timeseries during the spatial averaging
185 process. This would have a similar weighting effect to that of the corresponding spatially
186 averaged tide gauge stations that were close to each other with a similar sea level signal.



187

188 **Figure 3** Distribution of the 285 tide gauge bins where the CMEMS altimetry data (1993 to
189 2020) coincides with binned tide gauge observations (1901 to 2020) that are used for
190 our EOF reconstructions.

191

192



193 *2.3 Wind dataset and Southern Oscillation Index*

194 Previous work has shown that wind and climate indices play important roles in sea level
195 variability, for example, Calafat et al. (2018); Han, et al. (2017) and The Climate Change
196 Initiative Coastal Sea Level Team (2020). Here, we aim to assess whether Signal Differences
197 can be explained by wind forcing or climate indices. Because the EOF reconstruction is based
198 on successive differences, this is what we use to define the Signal Differences rather than sea
199 levels. For the wind analysis, we use monthly 10 m wind u and v components from the ERA5
200 reanalysis (Hersbach, et al., 2023), which are provided at $\frac{1}{4}^\circ$ resolution and were downloaded
201 from the Copernicus Climate Change Service, Climate Data Store website. The monthly wind
202 data had the annual and semi-annual cycles removed using harmonic analysis at each grid point,
203 and were then averaged in yearly values and detrended.

204 Wind u and v components were extracted within a 200 km radius from each individual tide
205 gauge station. Successive differences were then applied to identify the grid point with the
206 highest correlations between Signal Differences and the wind (u, v) timeseries. The wind (u,
207 v) timeseries at the point of maximum correlation were then spatially averaged within each tide
208 gauge bin and successive differences applied.

209 The second dataset was a climate index called the Southern Oscillation Index (SOI), a
210 normalized pressure difference between Tahiti and Darwin (Ropelewski and Jones, 1987),
211 which was downloaded from the University of East Anglia, Climatic Research Unit website.
212 This dataset was yearly averaged and successive differences applied for consistency. The SOI
213 was used as Calafat et al. (2014) commented that the El Niño–Southern Oscillation (ENSO)
214 signal was not captured properly because the EOF0 was used in the GMSL reconstructions.

215

216 *2.4 EOF Reconstruction*



217 For simplicity, the term *tide gauge bins* hereinafter are referred to as *tide gauges*. Calafat et al.
218 (2014) demonstrated that, in EOF reconstructions that include an EOF0, the reconstructed
219 GMSL can be expressed as a generalized weighted mean of the tide gauge records.

220

$$221 \quad GMSL = \sum_{i=1}^N w_i t_i \quad (1)$$

222 where $w = \frac{1^T \Sigma^{-1}}{1^T \Sigma^{-1} 1}$ and

223 Σ is the covariance matrix of altimetry records at tide gauge locations and is diagonally loaded
224 with the observational error.

225 w_i is the weight associated with the i -th tide gauge.

226 N is the total number of tide gauges available at each time step i .

227 1 is an $N \times 1$ column vector of ones.

228

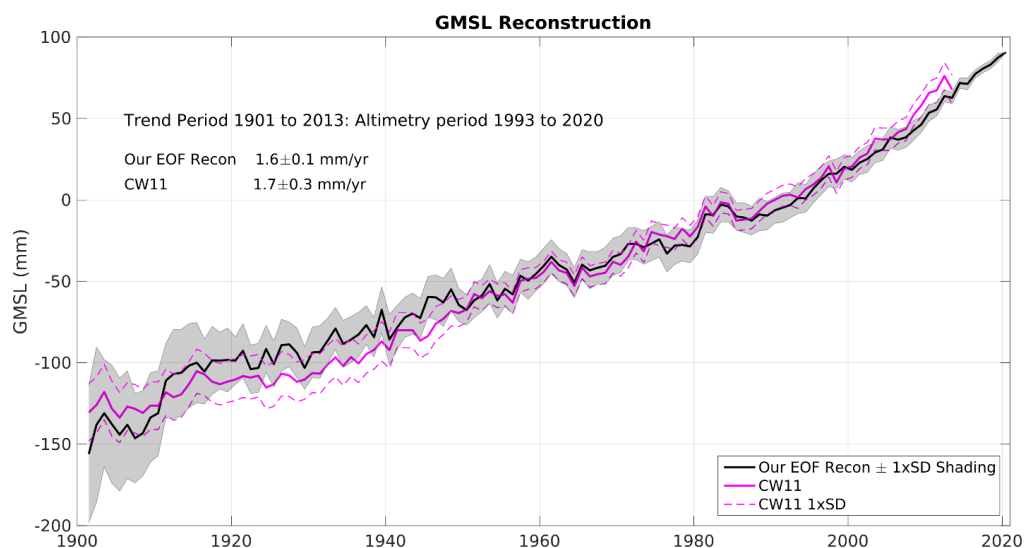
229 This is the formulation that we use in this study, but we remark that such formulation is
230 completely equivalent to that of CW11. Eq. (1) is applied to annual data with an observational
231 error of 2 cm.

232

233 As a sanity check, we reconstructed GMSL using the CMEMS global dataset (1993 to 2020)
234 and tide gauges (Fig. 3) and compared it with the GMSL reconstruction of CW11 (Fig. 4). The
235 trend from our GMSL reconstruction for the period 1901-2013 is 1.6 ± 0.1 mm/yr whereas that
236 from CW11's reconstruction is 1.7 ± 0.3 mm/yr, reflecting a very good agreement when
237 considering their uncertainty estimates (which account for serial correlation). The two
238 reconstructions agree also very well in terms of the variability with a correlation of 0.80 for
239 detrended time series (1910 to 2013), although there is a small offset between the two GMSL
240 curves between 1910 and 1950. If we expand the timeseries from 1901 to 2013 then the



241 correlation is reduced to 0.55. The uncertainty (shaded region) is quite large from 1901 to 1910
242 compared with the later period of the GMSL reconstruction, so it is not surprising that the
243 correlation had reduced between the two reconstructions. The uncertainty ($\pm 1\sigma$) in the GMSL
244 trends is estimated using a regression model with serial correlation errors, in order to obtain
245 more realistic error estimates (Chib, 1993).



246

247 **Figure 4** Comparison of our EOF reconstruction (black) derived from Eq. (1) with that of
248 CW11 (magenta). The shaded area (grey) represent the 1-sigma uncertainty interval,
249 which reflects the sensitivity of the reconstruction to the number of tide gauge bins as
250 evaluated Standard deviation (SD) using a bootstrap method.

251

252 *2.5 Multiple Linear Regression Model for Signal Differences*

253

254 As discussed earlier, the low ability of EOF reconstructions to capture the GMSL variability
255 appears to be largely due to differences between the tide gauges and the corresponding
256 altimetry data (i.e., the Signal Differences). Hence, if we were able to build a regression model



257 for the Signal Differences with good predictive skill, this would enable us to improve the
258 reconstruction of the GMSL variability by adjusting the tide gauge data prior to the
259 reconstruction which includes tide gauge observations before 1993. To this end, we will begin
260 by investigating the relationship between the Signal Differences and plausible predictors such
261 as wind, a climate index (Southern Oscillation Index) and the tide gauge record itself. The
262 reason for including the tide gauge record as a predictor is to account for the possibility that
263 the Signal Differences could be due to a simple scale factor between the altimetry and the tide
264 gauge time series, or to local coastal signals unobserved by altimetry. To select the regression
265 predictors, we performed an exploratory correlational analysis involving the Signal Differences
266 and the plausible predictors listed above. Such analysis is based on detrended yearly timeseries
267 with the successive differences applied.

268

269 Using these predictors, we designed three Signal Differences multiple linear regression models
270 Eq. (2 to 4) to be associated with each tide gauge. Model 1, Eq. (2) uses the wind u and v
271 components as the predictors, followed by the addition of the SOI, Eq. (3) and tide gauge
272 observation (TG, Eq. 4) sequentially. We tested the regression Models at each tide gauge by
273 analyzing the correlations between the Signal Differences and the regression Models, and also
274 their corresponding explained variance. It is important to note here these multiple regression
275 models are designed to predict the Signal Differences rather than explaining their origin, thus
276 we are not concerned whether the predictors are correlated.

277

$$278 \quad \text{Signal Differences}_{\text{Model 1}} = a + b_1 \text{Wind}_u + b_2 \text{Wind}_v \quad (2)$$

279

$$280 \quad \text{Signal Differences}_{\text{Model 2}} = a + b_1 \text{Wind}_u + b_2 \text{Wind}_v + b_3 \text{SOI} \quad (3)$$

281



282 $Signal\ Differences_{Model\ 3} = a + b_1 Wind_u + b_2 Wind_v + b_3 SOI + b_4 TG$ (4)

283

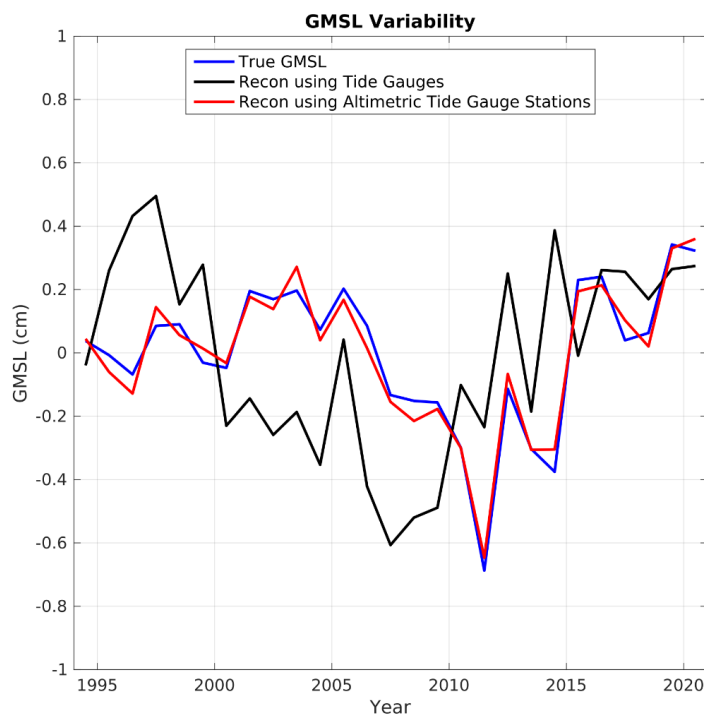
284 **3. Results**

285 We start by comparing our uncorrected GMSL reconstruction with the ‘true’ GMSL from
286 altimetry for the period 1994 to 2020 (Fig. 5). The variability in the two time series is fairly
287 different, with a correlation of 0.23. The SD of our reconstruction was 0.31 cm and that of the
288 ‘true’ GMSL was 0.23 cm. Next, we compute a second GMSL reconstruction by replacing the
289 tide gauges with the corresponding altimetry time series (virtual altimetric tide gauges). Note
290 that in this second reconstruction, the Signal Differences are exactly zero by construction. In
291 this case, the GMSL reconstruction is almost a perfect match to the ‘true’ GMSL variability
292 (Fig. 5), with a correlation of 0.98. These results strongly support the statement that we made
293 in the Introduction that differences between tide gauges and the corresponding altimetry data
294 lead to a significant shortfall in the skill of EOF reconstructions that include an EOF0. They
295 also suggest that we can potentially improve the skill of the EOF reconstructions by adjusting
296 such differences prior to conducting the reconstruction..

297

298 The next stage of this study is to investigate if these Signal Differences have any spatial
299 structure that can be exploited to build a regression model of the Signal Differences. This would
300 then allow us to remove the Signal Difference from the tide gauge data, potentially leading to
301 a better GMSL reconstruction.

302



303

304 **Figure 5** Comparison between the true GMSL and our GMSL reconstructions using tide gauge
305 observations (black line) and virtual altimetric tide gauges (red line) for the period 1994
306 to 2020. The ‘true’ GMSL derived from altimetry is shown as a blue line. All timeseries
307 are detrended.

308

309 *3.1 Signal Differences*

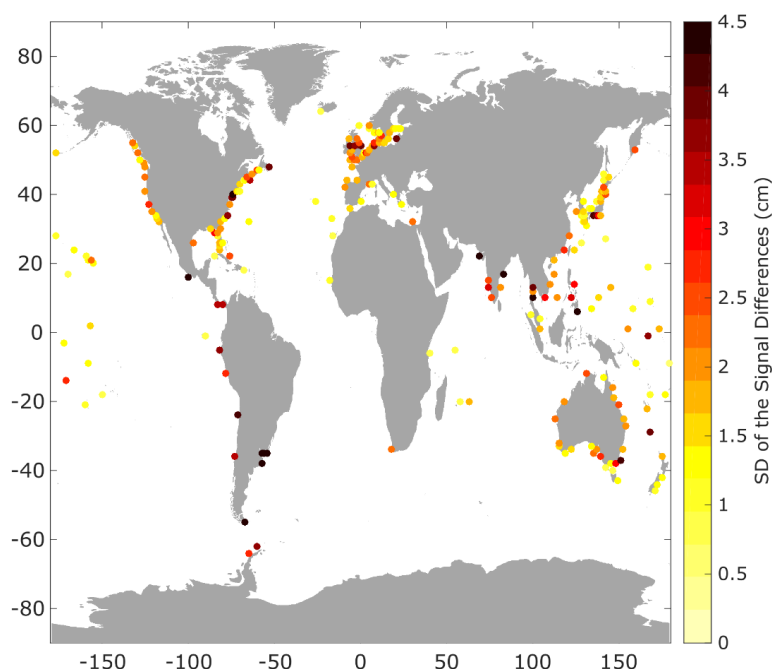
310

311 Recall that the Signal Differences are defined as the difference between each binned tide gauge
312 location and its corresponding binned altimetry observations where both the tide gauge and
313 altimetry data had the successive differencing applied.

314



315 We begin by showing the SD of the Signal Differences for the period 1994 to 2020 using 229
316 tide gauge (Fig. 6). The original 285 locations from the tide gauge dataset were subsampled to
317 229 locations where the data covered at least eight years, so that we could maximize the number
318 of locations to estimate reliable correlations and SDs of the Signal Differences. Of the 229
319 locations in the subsample, most (90%) contained at least 16 years of data.



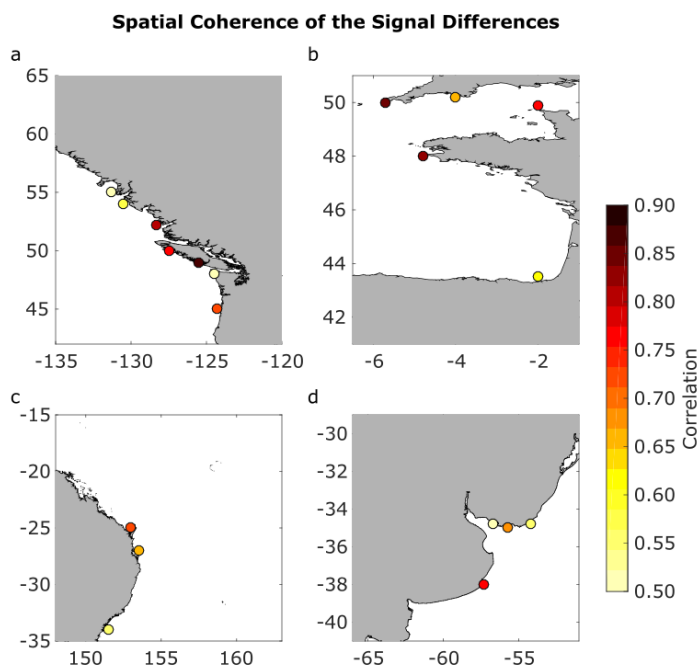
320 **Figure 6** The Standard Deviation (SD) of the Signal Differences

321

322 The spatial distribution of the Signal Differences shows SD values ranging from almost 0 to
323 4.5 cm where clusters of medium to high values (>2 cm) are generally found along continental
324 coastlines and low values (<1.5 cm) found along both continental coastlines and islands within
325 the open ocean (Fig. 6). This provides some evidence of spatial structure (coherency) within
326 the Signal Differences data. To further quantify the coherence of the Signal Differences, we
327 correlate the Signal Differences from individual sites with the average of the Signal Differences
328 over all sites within four different regions, namely the west coast of North America, the Bay



329 of Biscay/English Channel, North East Australia, and South America (Fig. 7). The average
330 correlation for each region is, respectively 0.68 (SD 0.15), 0.74 (SD 0.11), 0.65 (SD 0.08) and
331 0.62 (SD 0.12). The correlation values are not completely uniform within each region, but this
332 is likely due to unique localised physical mechanisms (such as bathymetry; local vertical
333 movement; ocean currents; wind; etc) that may affect these differences between the tide gauge
334 and altimetry observations. These correlations are high enough to conclude that the Signal
335 Differences are not random but rather due to coastal signals not captured by altimetry and/or a
336 scale factor between the tide gauge and altimetry measurements. Indeed, if we replace all the
337 Signal Differences in Fig. 7a (i.e.7 tide gauges) with random values and repeat the analysis
338 100,000 times, then the mean correlation is 0.37, much lower than what we find in reality.



339 **Figure 7** The spatial coherence of the Signal Differences in the west coast of North America
340 (a); the Bay of Biscay (b); northeast Australia (c) and the Río de la Plata basin
341 Argentina/Uruguay (d). The correlations are significant at the 95% Confidence Interval
342 (CI).



343 We examine the nature of the Signal Differences further by correlating, at each tide gauge: 1)
344 the time series from tide gauges and altimetry (Fig. 8a); 2) the Signal Differences with the tide
345 gauge time series (Fig. 8b); and 3) the Signal Differences with the altimetry time series (Fig.
346 8c). From a total of 229 tide gauges, 204 bins had a significant correlation (at the 95% CI)
347 between tide gauge and CMEMS altimetry, with an average correlation of 0.82 (Fig. 8a). In
348 general, high correlations between tide gauges and altimetry show low SDs of Signal
349 Differences, especially in the central and western Pacific Ocean. This indicates that, in general,
350 the Signal Differences is due to signals that are observed by one of the instruments (either the
351 tide gauge or altimetry) but not the other. Note, however, that a high correlation does not always
352 mean that there is a low Signal Differences as there may be a scale factor between the altimetry
353 and the tide gauge time series. There are a few locations (including the south-east and west
354 coasts of South America and the southern west coast and northeast coast of Great Britain) that
355 show correlation values between 0.4 to 0.6. These lower correlation values coincide with higher
356 SD values of the Signal Differences.

357

358

359

360

361

362

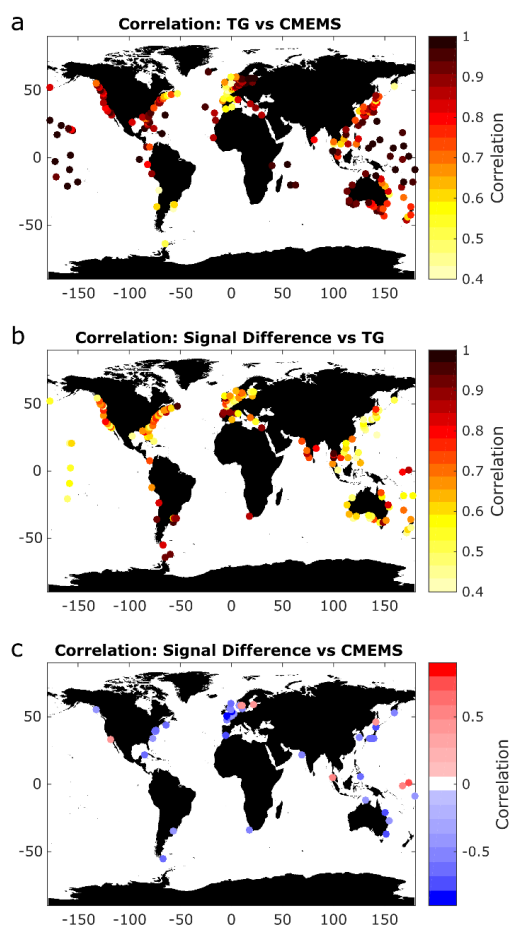
363

364

365

366

367



368

369 **Figure 8** Correlations between tide gauge and CMEMS altimetry (a); between the Signal
370 Differences and tide gauges (b); and between Signal Differences and CMEMS altimetry
371 (c). Only correlations that are statistically significant at the 95% CI are shown.

372

373 A total of 146 (out of 229) locations had a statistically significant correlation between tide
374 gauge observations and their corresponding Signal Differences (Fig. 8b), whereas only 45
375 locations had significant correlations between altimetry and Signal Difference (Fig. 8c). If we
376 break this down further, 119 locations had significant correlations of Signal Differences with



377 tide gauge observations only; 18 locations had a significant correlation with altimetry only; and
378 finally, 27 locations had a significant correlation with both the tide gauge and altimetry
379 observations. In summary, a total of 164 locations out of 229 had a significant correlation with
380 the Signal Differences (i.e. $119_{TG} + 18_{CMEMS} + 27_{TG \& CMEMS} = 164$).

381

382 The fact that Signal Differences at most locations are correlated with tide gauges but not with
383 altimetry tells us something important: that signals detected by the tide gauges but not observed
384 by altimetry are contributing to the Signal Differences (Fig. 8b & c). It is not surprising that
385 the significant correlations between Signal Differences and altimetry observations displayed in
386 Fig. 8c are mostly negative because the Signal Differences are defined as tide gauge minus
387 altimetry. The central and western Pacific Ocean and western Indian Ocean show low SD of
388 the Signal Differences (Fig. 6) with high correlation between the tide gauge and altimetry (Fig.
389 8a), yet few significant correlations between the Signal Differences and either tide gauge or
390 altimetry (Fig. 8b and c). This tells us that both sensors are seeing the same sea level signal in
391 these regions. Moreover, if a large SD Signal Differences are observed at tide gauge where the
392 correlation between altimetry and tide gauges is very high, then this should be largely due to a
393 scale factor between the altimetry and tide gauge time series. In this case, the Signal
394 Differences should be highly correlated to both the tide gauges and the altimetry. This is
395 observed in 16 out of the 27 $TG \& CMEMS$ grouped locations (half of which are in the
396 north/northwest of Europe) that had a significant correlation between tide gauge and altimetry
397 with a corresponding mean SD of the Signal Differences of 2.1 cm.

398

399 The southern west coast of South America is intriguing. Here, there are high SDs of Signal
400 Differences (Fig. 6), with significant correlations between tide gauge and altimetry, (i.e., 0.4
401 to 0.6) but no significant correlations between Signal Differences and altimetry. This implies



402 that the tide gauge observations are detecting something that the altimeter does not, even
403 though the correlations between tide gauge and altimetry are significant.

404

405 Western Australia and west coast of Central America are similar to the west coast of South
406 America except that the correlations between the tide gauges and altimetry in Western Australia
407 and west coast of Central America are very strong compared with South America. This high
408 correlation can occur even if the SDs of the Signal Differences are high, such as when both tide
409 gauge and altimetry observations are picking up the same sea level signal but with different
410 amplitudes, leading to higher Signal Differences.

411

412 *3.2 Relationship of the Signal Differences with Wind and the ENSO*

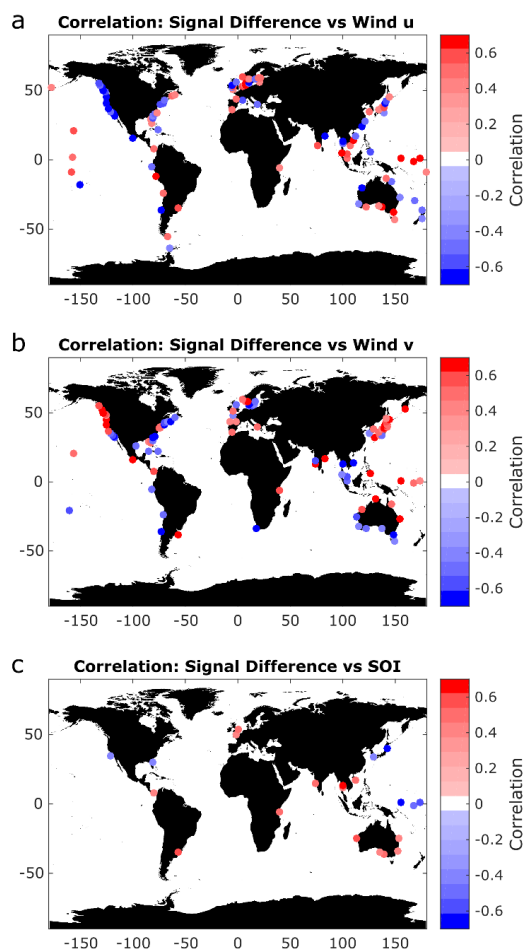
413

414 So far, we have shown that the Signal Differences are not due to random instrumental errors,
415 and thus it may be explained through external factors (components) such as atmospheric
416 forcing on sea level. For many decades researchers have investigated wind as a contributing
417 factor, influencing sea level changes along the coasts (e.g. Calafat et al., 2018; Gill and Clarke,
418 1974; Piecuch et al., 2016; Johansson *et al.*, 2022; Sturges and Douglas, 2011 and The Climate
419 Change Initiative Coastal Sea Level Team, 2020). Here we correlate the Signal Differences
420 with the zonal and meridional components of the, u and v (Fig. 9a and b, respectively).
421 Globally, there are strong coherent spatial patterns of correlations (both positive and negative)
422 between the Signal Differences and wind (u,v), with absolute correlation values of 0.5 or more
423 at many locations. The Pacific coast of the US, Australia, the UK and Japan are regions that
424 show particularly coherent structures, whereas in the west and central Pacific Ocean the wind
425 appears to be less of a factor to explain the Signal Differences.

426



427



428 **Figure 9** Correlations between the Signal Differences and wind u parameter (a); between the
429 Signal Differences and wind v (b); and between the Signal Differences and the Southern
430 Oscillation Index (SOI) (c). Only correlations that are statistically significant at the 95%
431 CI are shown.

432

433 Another factor that could explain the Signal Differences is sea-level variability associated with
434 the ENSO, particularly in the Pacific Ocean, as this has been shown to play an important role
435 in the interannual climate variability (Han et al., 2017; Hamlington et al., 2020; McPhaden et



436 al., 2006; Nerem et al., 2010; Royston et al., 2018 and Zhang and Church, 2012). Calafat et al.
437 (2014) also showed that the ENSO influence on GMSL is not well captured by EOF
438 reconstructions that use the EOF0. Here, we correlate the annual SOI climate index with the
439 Signal Differences and found significant correlations at many tide gauge locations, implying
440 that the Signal Differences has an SOI component (Fig. 9c). In most cases, the significant
441 correlations were positive along many coastlines, with the exceptions of a few coherent clusters
442 of negative correlations to the northeast of Papua New Guinea, Japan and southern USA. To
443 some extent, the correlations with the SOI index might reflect the effects of local wind forcing
444 on sea level, but they could also indicate a contribution from remote atmospheric forcing
445 associated with the ENSO.

446

447 *3.3 Multiple Linear Regression for the Signal Differences (1994-2020)*

448

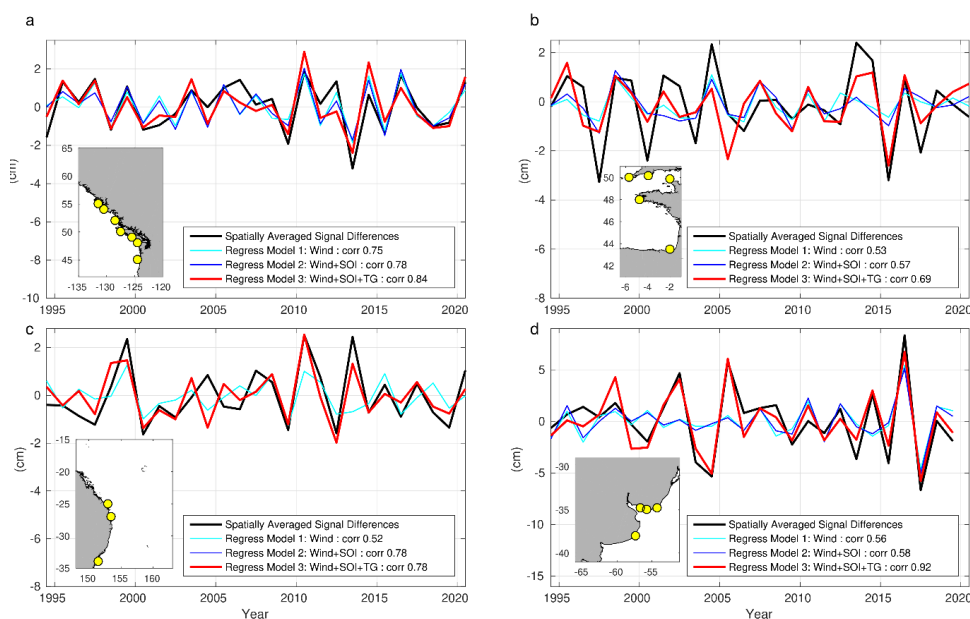
449 The significant correlations that we have found of wind and SOI parameters against the Signal
450 Differences in many regions provide the basis to create a multiple linear regression model that
451 includes these variables. Here, we investigate three multiple linear regression models (Models
452 1 to 3, Eq. 2 to 4)

453

454 To assess the performance of the three regression models, we begin by focusing on the same
455 four regions (Fig. 7) that showed strong regional coherence of the Signal Differences (i.e., west
456 coast of North America, the Bay of Biscay/English Channel, Northeast Australia, and South
457 America). We correlate the prediction of the regression model with the Signal Differences,
458 both averaged over the corresponding region. Fig. 10 shows that the wind plays an important
459 role in explaining a large part of the Signal Differences in all four regions, with correlations
460 between the Signal Differences and Model 1 ranging from 0.52 to 0.75. Progressively adding



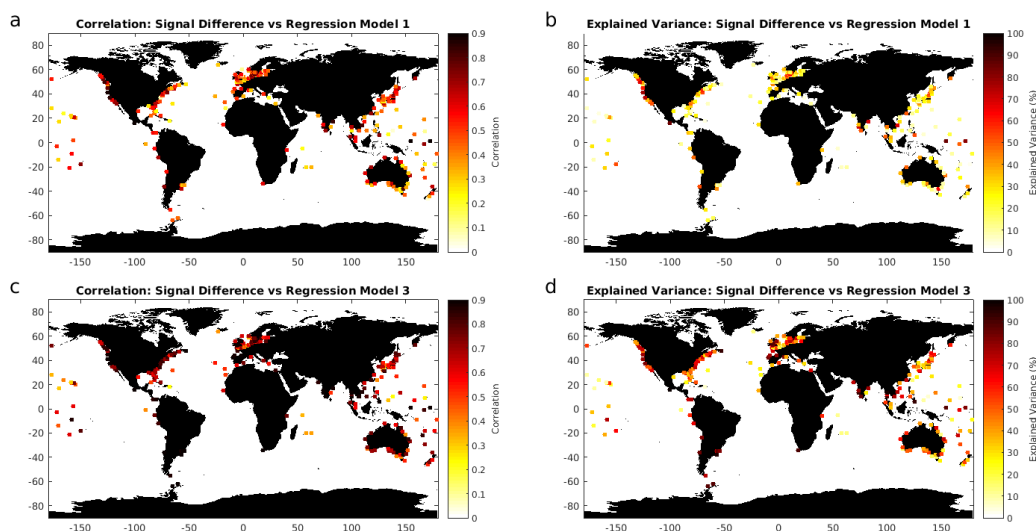
461 the SOI and the tide gauge parameter (Models 2 and 3) generally improves the correlation and
462 scale factor, although to a lesser extent and with regional variation in correlations. Please note
463 that the regression Model 2 (blue line in Fig. 10c) appears to be missing because the regression
464 Model 3 (red line) has superimposed itself on the regression Model 2. This is reflected as the
465 correlation between spatially averaged Signal Differences and regression Models 2 and 3 have
466 the same correlation of 0.78.



467
468 **Figure 10** Time series of spatially averaged Signal Differences from the tide gauge within each
469 region (insert) compared with the time series from the three regression models, for the
470 west coast of North America (Washington State and British Columbia,(a); Bay of
471 Biscay/English Channel (b); northeast Australia (c) and the Río de la Plata basin
472 Argentina/Uruguay (d). These regions are the same as Fig. 7.
473



474 We have also assessed the performance of Model 1 and Model 3 at each of the 285 tide gauges
475 by computing the correlation and the explained variance (Fig. 11). Model 1 (only wind) shows
476 a globally averaged correlation with the Signal Differences of 0.48 and an average explained
477 variance of 27%. The highest correlation values are found along the west coasts of North
478 America, India and Australia (Fig. 11 a, b). Model 3 (wind, SOI and TG as predictors) show
479 significantly higher correlations and explained variance, with globally averaged values of 0.68
480 and 50% (Fig. 11 c, d), respectively.



481

482 **Figure 11** The correlations (a) between the Signal Differences and the regression Model 1, Eq.

483 (2) and the corresponding explained variance (b). The correlations (c) between the

484 Signal Differences and the regression Model 3, Eq. (4) and the corresponding explained

485 variance (d).

486

487

488

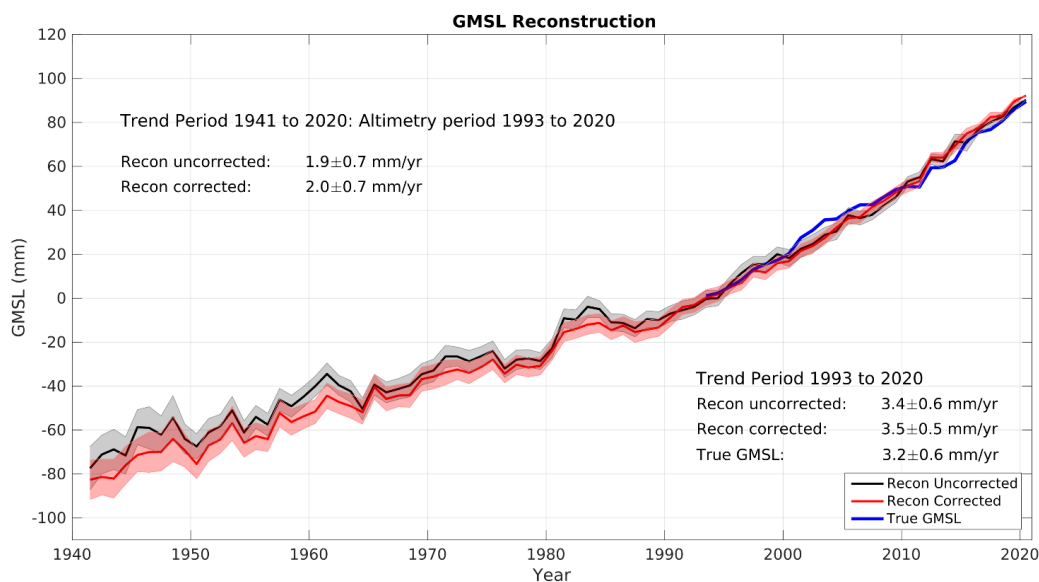


489 *3.4 Adjusting the Tide Gauge Observations prior to GMSL Reconstruction using the Signal*

490 *Differences Multiple Linear Regression Model*

491

492 Here, we use regression Model 3 to correct for the Signal Differences at each tide gauge from
493 1941 to 2020 prior to computing the EOF reconstruction. To do this, we first derive the Model
494 3 parameters using the period from 1994 to 2020 where both the wind (u,v) and the tide gauge
495 predictors were detrended prior to computing the EOF reconstruction and then the Signal
496 Differences were determined at each tide gauge and were also extrapolated back in time (1941
497 to 1993). The corrected EOF reconstruction compared with our uncorrected reconstruction as
498 well as the ‘true’ GMSL (1993 to 2020) from the altimetry period are shown in Fig. 12. The
499 trends for both the uncorrected and corrected EOF reconstruction are statistically the same,
500 1.9 ± 0.7 mm/yr, 2.0 ± 0.7 mm/yr, respectively. For the altimetry period (1993 to 2020) the trends
501 show that uncorrected EOF reconstruction (3.4 ± 0.6 mm/yr); corrected reconstruction (3.5 ± 0.5
502 mm/yr) and the ‘true’ GMSL trend (3.2 ± 0.5 mm/yr) are also statistically the same. This means
503 that the trends are not influenced by the Signal Differences correction.



504

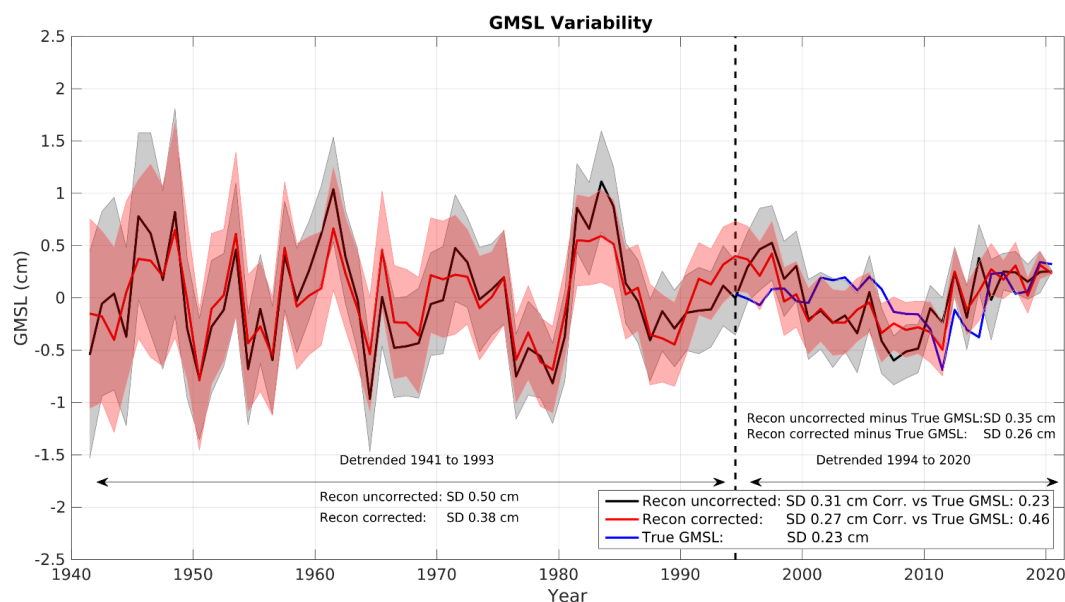
505 **Figure 12** Comparison of uncorrected EOF reconstruction (black line) derived from Eq. (1)
506 and the corrected EOF reconstruction (red line). The 1-sigma uncertainty intervals,
507 shaded grey and light red respectively, reflect the sensitivity of the reconstruction to the
508 number of tide gauges as evaluated SD using a bootstrap method. The ‘true’ GMSL
509 derived from altimetry is shown as a blue line (1994 to 2020).

510

511 Focusing now on the reconstructed variability (Fig. 13), both the uncorrected and corrected
512 reconstruction of GMSL show in general a reduction in the later period (1994-2020) compared
513 with the earlier period (1941-1993). We find that for the earlier period, the corrected EOF
514 reconstruction displays reduced variability compared with the uncorrected reconstruction, with
515 SDs of 0.38 cm and 0.50 cm, respectively. For the later period, we can also include the ‘True’
516 GMSL from altimetry in the comparison. The corrected GMSL reconstruction shows a
517 significantly higher correlation with the true GMSL with a value of 0.46, compared with 0.23
518 for the uncorrected reconstruction. The magnitude of the GMSL variability is also better



519 captured by the corrected reconstruction, as quantified by the SD of the time series, which is
520 0.27 cm and 0.31 cm for the corrected and uncorrected reconstructions, respectively, compared
521 to a SD of 0.23 cm for the true GMSL. The difference between our uncorrected reconstruction
522 and the true GMSL shows a SD of 0.35 cm, whereas the difference between the corrected
523 reconstruction and the true GMSL gives a SD of 0.26 cm. This implies a reduction of 26% in
524 the error associated with the reconstruction of the GMSL variability.



525

526 **Figure 13** The variability of the GMSL that has been detrended for two time periods 1941 to
527 1993 and 1994 to 2020 showing the uncorrected EOF reconstruction (black line)
528 derived from Eq. (1) and the corrected EOF reconstruction (red line). The 1-sigma
529 uncertainty intervals shaded grey (uncorrected) and light red (corrected) reflect the
530 sensitivity of the reconstruction to the number of tide gauges as evaluated standard
531 deviation (SD) using a bootstrap method. The detrended 'true' GMSL derived from
532 altimetry is shown as a blue line (1994 to 2020).

533



534 The earlier period in Fig. 13 had a larger uncertainty for both reconstructions (shaded regions)
535 compared with the later period, most likely due to the smaller number of tide gauges compared
536 with the later time period. The uncertainties of the uncorrected and corrected EOF
537 reconstruction for the earlier period were similar except for the very strong 1983-1984 El Niño
538 event where the corrected uncertainty was reduced. The later period generally shows a
539 reduction of corrected uncertainty compared with uncorrected uncertainty, especially during
540 the very strong El Niño events of 1997-1998 and 2015-2016. In addition, the later period shows
541 that the corrected reconstruction (red line) lies closer to the true altimetry GMSL (blue line)
542 for both of these very strong El Niño events. This does imply that uncorrected GMSL
543 reconstruction did not capture ENSO events well.

544

545 **4. Discussion and Conclusion**

546

547 This study has shown that the use of EOF reconstruction to estimate GMSL variability is
548 improved by adjusting the tide gauge observations for the Signal Differences prior to the EOF
549 reconstruction. We found initially that the Signal Differences between the tide gauge
550 observations and the altimetry data show regional spatial coherence along the coasts (e.g. Fig.
551 6 and 7). Furthermore, such differences are significantly correlated with tide gauges at most
552 locations, but often not with altimetry (Fig. 8), which rules out observation errors as the cause
553 of the differences. This suggests instead that the differences are due to real oceanographic
554 signals that are not adequately captured by altimetry. The significant correlations (at 95% CI)
555 between the Signal Differences with wind and SOI globally (Fig. 9) enabled us to build Signal
556 Differences multiple linear regression models at each tide gauge. Here, the Wind and SOI
557 variables were used as predictors as part of the linear regression models to predict these Signal
558 Differences before 1993, which are then applied to the tide gauge observations prior to the



559 GMSL reconstruction, generating a corrected GMSL reconstruction. Model 3, Eq. (4) was
560 found to be the most appropriate both regionally (Fig.10) and globally (Fig. 11). A large
561 fraction of the Signal Differences has been explained by wind forcing and/or the tide gauge
562 data themselves through multiple linear regression. Although the SOI played a minor role in
563 the regression model, it did play an important role in the northeast Australian region (Fig. 9c
564 and 10c) as this area is influenced by the ENSO and is consistent with White et al., (2014).

565

566 The corrected GMSL reconstruction shows improved GMSL variability (Fig. 13), with a
567 correlation of 0.46 compared with 0.23 for the uncorrected reconstruction. The corrected
568 GMSL reconstruction also shows reduced variability than the uncorrected reconstruction, thus
569 showing a better agreement with the true GMSL from altimetry. The GMSL variability was
570 greater during the earlier period for both the uncorrected and corrected reconstruction although
571 there was a reduced SD for the latter. The large uncertainty from the uncorrected GMSL
572 reconstruction in Fig. 13 (shaded grey) corresponds with El Niño events (including the very
573 strong events in 1982-1983, and 2015-2016) compared with the corrected GMSL
574 reconstruction (shaded red), providing evidence that the uncorrected GMSL reconstruction did
575 not capture ENSO well.

576

577 In some regions both the tide gauge and altimetry observations are detecting the same sea level
578 signal. A lot of island tide gauge locations in the central Pacific Ocean straddle the Doldrums
579 (5°S to 5°N), which has little wind. Beyond the latitudes of the Doldrums, the trade winds are
580 a dominant feature and Yang et al. (2022) showed an acceleration in trade winds in the mid to
581 late 1990s. It is not surprising that there is a strong correlation between tide gauge and altimetry
582 because the sea level signal has a lack of wind or a stable large scale trade wind component
583 that the altimeter also detects. However, not all Pacific islands followed this trend, as a few



584 locations had a significant correlation between Signal Differences with wind (Fig. 9) and had
585 a low or medium magnitude of the Signal Differences. No significant correlation between
586 Signal Differences and altimetry were shown at these island sites (Fig. 8c) implying that these
587 locations have some sea level signal, such as the wind component, that the altimetry did not
588 capture or other physical mechanisms contributing to the difference in sea level variability in
589 the region (e.g. The Climate Change Initiative Coastal Sea Level Team, 2020). Thus, more
590 understanding of the atmospheric and oceanographic processes can lead to other factors that
591 may influence the Signal Differences, providing an improved regression model.

592

593 Future advancements to the Signal Differences regression model beyond this study will be to
594 investigate the locations where the magnitude of Signal Differences is low and determine if
595 these locations are necessary for a Signal Differences regression model to be applied. As
596 previously mentioned, this study assumed that the regression coefficients are constant with
597 time (1994 to 2020), but this temporal stability becomes important for a Signal Differences
598 model to be applied to tide gauge data prior to 1993. Temporal sensitivity testing during the
599 altimetry period provides a good starting point for future altimetry development by targeting
600 these regions where the Signal Differences are seen by the tide gauge observations but not by
601 the altimeter. In addition, further work can investigate other coastal processes that contribute to
602 the Signal Differences beyond the local wind and SOI climate index found here, such as the
603 effects of river discharge in local and regional sea level variability (Piecuch et al., 2018).
604 Piecuch (2023) pointed out that there may be implications for twentieth-century GMSL
605 reconstructions as the river effects on tide gauges such as in the Río de la Plata should be
606 removed prior to GMSL reconstruction.

607



608 In conclusion, the differences between tide gauges and altimetry (Signal Differences) are
609 significantly correlated along the coast, and these differences are correlated well with local
610 winds, and it appears that this is not always adequately captured by altimetry. The over
611 estimation in variability of the GMSL EOF reconstruction has been shown to be reduced by
612 applying a Signal Differences correction model to the tide gauge observations prior to
613 reconstruction. Correcting the Signal Differences as a first step through the regression model
614 (Model 3) prior to the reconstruction reduces the SD of the reconstructed GMSL variability by
615 26% and significantly increases the correlation with observed altimetry GMSL (1994-2020).
616 The Signal Differences were extrapolated prior to 1993 which showed the corrected EOF
617 GMSL reconstruction variability also had reduced uncertainty compared with the uncorrected
618 reconstruction. Caution is needed as the Signal Differences at a tide gauge may not be due to a
619 physical oceanographic signal but instead just bad altimetry data, tide gauge data or both.

620

621

622

623



624 **Code availability**

625 All figures were created with MATLAB software. Some maps used the Global Self-consistent
626 Hierarchical High-resolution Shorelines (GSHHS; Wessel and Smith, 1996).

627

628 **Data availability**

629 All data are freely available from data providers that is explained in detail in the Data and
630 Methods section of the paper.

631

632 **Author contribution**

633 AS quality controlled the data, performed analysis, created the figures, interpreted the results,
634 wrote the original draft and reviewed and edited the manuscript. SJ, contributed to project
635 management, funding acquisition, and the review and editing of the manuscript. FC proposed
636 the study, funding acquisition, supervision, methodology, project management and the review
637 and editing of the manuscript. SJ and FC also provided advice on the analysis of the study.

638

639 **Competing interests**

640 The authors declare that they have no known competing financial interests or personal
641 relationships that could have appeared to influence the work reported in this paper.

642

643 **Acknowledgements**

644 We are grateful for Chis Banks from the National Oceanography Centre, Liverpool, U.K. for
645 his help and advice.

646

647



648 **Financial support**

649 The authors gratefully acknowledge funding from the European Space Agency that supported
650 this phase of the Climate Change Initiative (CCI) for the Sea level CCI + phase two for the
651 Coastal Sea Level program. S.J was supported by NERC NC International programme: Future
652 states of the global Coastal ocean: Understanding for Solutions (FOCUS: NE/ X006271/1) and
653 NC AtlantiS funding (NE/ Y005589/1)

654

655 **References**

656

657 Calafat FM, Chambers DP, MN Tsimplis (2014). On the ability of global sea level
658 reconstructions to determine trends and variability. *Journal of Geophysical Research:*
659 *Oceans* 119 (3), 1572-1592. <https://doi.org/10.1002/2013JC009298>

660 Calafat FM and D Gomis (2009). Reconstruction of Mediterranean sea level fields for the
661 period 1945–2000. *Global and Planetary Change* 66 (3-4), 225-234.
662 <https://doi.org/10.1016/j.gloplacha.2008.12.015>

663 Calafat, F.M., Wahl, T., Lindsten, F. *et al.* (2018). Coherent modulation of the sea-level annual
664 cycle in the United States by Atlantic Rossby waves. *Nat Commun* 9, 2571
665 <https://doi.org/10.1038/s41467-018-04898-y>

666 Chib, S. 1993. Bayes regression with autoregressive errors: A Gibbs sampling approach.
667 *Journal of Econometrics*, 58, 275-294. [https://doi.org/10.1016/0304-4076\(93\)90046-8](https://doi.org/10.1016/0304-4076(93)90046-8)

668 Church, J. A., and N. J. White (2006), A 20th century acceleration in global sea-level rise,
669 *Geophys. Res. Lett.*, 33, L01602, doi:10.1029/2005GL024826.

670 Church, J. A., and N. J. White (2011), Sea-level rise from the late 19th to the early 21st Century,
671 *Surv. Geophys.*, 32, 585–602, doi:10.1007/s10712-011-9119-1.



- 672 Church, J. A., N. J. White, R. Coleman, K. Lambeck, and J. X. Mitrovika (2004), Estimates of
673 the regional distribution of sea level rise over the 1950–2000 period, *J. Clim.*, 17, 2609–
674 2625.
- 675 Christiansen, B., T. Schmith, and P. Thejll (2010), A surrogate ensemble study of sea level
676 reconstructions, *J. Clim.*, 23, 4306–4326, doi:10.1175/2010JCLI3014.1.
- 677 Cipollini, P., Calafat, F.M., Jevrejeva, S.*et al* (2017). Monitoring Sea Level in the Coastal Zone
678 with Satellite Altimetry and Tide Gauges. *Surv Geophys* 38, 33–57
679 <https://doi.org/10.1007/s10712-016-9392-0>
- 680 Compo, G.P., Whitaker, J.S., Sardeshmukh, P.D., Matsui, N., Allan, R.J., Yin, X., Gleason,
681 B.E., Vose, R.S., Rutledge, G., Bessemoulin, P., Brönnimann, S., Brunet, M.,
682 Crouthamel, R.I., Grant, A.N., Groisman, P.Y., Jones, P.D., Kruk, M.C., Kruger, A.C.,
683 Marshall, G.J., Maugeri, M., Mok, H.Y., Nordli, Ø., Ross, T.F., Trigo, R.M., Wang,
684 X.L., Woodruff, S.D. and Worley, S.J. (2011), The Twentieth Century Reanalysis
685 Project. *Q.J.R. Meteorol. Soc.*, 137: 1-28. <https://doi.org/10.1002/qj.776>
- 686 CMEMS Altimetry dataset, <https://marine.copernicus.eu/access-data>
- 687 Dangendorf, S., Hay, C., Calafat, F.M.*et al.* (2019). Persistent acceleration in global sea-level
688 rise since the 1960s. *Nat. Clim. Chang.* 9, 705–710. [https://doi.org/10.1038/s41558-019-](https://doi.org/10.1038/s41558-019-0531-8)
689 0531-8
- 690 Dangendorf, S., Frederikse, T., Chafik, L.*et al.* (2021). Data-driven reconstruction reveals
691 large-scale ocean circulation control on coastal sea level. *Nat. Clim. Chang.* 11, 514–
692 520. <https://doi.org/10.1038/s41558-021-01046-1>
- 693 Dangendorf, S., Hendricks, N., Sun, Q.*et al.* (2023). Acceleration of U.S. Southeast and Gulf
694 coast sea-level rise amplified by internal climate variability. *Nat Commun* 14, 1935.
695 <https://doi.org/10.1038/s41467-023-37649-9>



- 696 Gill, A. E., and A. Clarke (1974), Wind-induced upwelling, coastal currents and sea-level
697 changes, *Deep Sea Res.*, 21, 325–345.
- 698 Hamlington, B.D.; Frederikse, T.; Nerem, R.S.; Fasullo, J.T.; Adhikari, S. Investigating the
699 acceleration of regional sea level rise during the satellite altimeter era (2020).
700 *Geophys. Res. Lett.*, 47, e2019GL086528. <https://doi.org/10.1029/2019GL086528>.
- 701 Hamlington, B.D. Piecuch C.G. Reager, J.T. Chandanpurkar, H, Frederikse T.R., Nerem S.,
702 Fasullo, J.T. and S-H. Cheon (2020). Origin of interannual variability in global mean
703 sea level. *Earth, Atmos. and Planetary Sci*, 117 (25) 13983-13990.
704 <https://doi.org/10.1073/pnas.19221901>
- 705 Han, W.; Meehl, G.A.; Stammer, D.; Hu, A.; Hamlington, B.; Kenigson, J.; Palanisamy, H.;
706 Thompson, P. (2017). Spatial patterns of sea level variability associated with natural
707 internal climate modes. *Surv. Geophys.* 38, 217–250. [https://doi.org/10.1007/s10712-](https://doi.org/10.1007/s10712-016-9386-y)
708 [016-9386-y](https://doi.org/10.1007/s10712-016-9386-y).
- 709 Hersbach, H., Bell, B., Berrisford, P., Biavati, G., Horányi, A., Muñoz Sabater, J., Nicolas, J.,
710 Peubey, C., Radu, R., Rozum, I., Schepers, D., Simmons, A., Soci, C., Dee, D.,
711 Thépaut, J-N. (2023): ERA5 monthly averaged data on pressure levels from 1940 to
712 present. Copernicus Climate Change Service (C3S) Climate Data Store (CDS), DOI:
713 [10.24381/cds.6860a573](https://doi.org/10.24381/cds.6860a573) (Accessed on 15-08-2023)
- 714 Holgate, S.J. Matthews A., Woodworth, P.L. Rickards, L.J., Tamisiea, M.E., Bradshaw, E.,
715 Foden, P.R., Gordon, K.M., Jevrejeva, S. and J. Pugh (2013). New Data Systems and
716 Products at the Permanent Service for Mean Sea Level. *Journal of Coastal Research*:
717 Volume 29, Issue 3: pp. 493 – 504. doi:10.2112/JCOASTRES-D-12-00175.
- 718 IPCC, 2021: *Climate Change 2021: The Physical Science Basis. Contribution of Working*
719 *Group I to the Sixth Assessment Report of the Intergovernmental Panel on Climate*
720 *Change*[Masson-Delmotte, V., P. Zhai, A. Pirani, S.L. Connors, C. Péan, S. Berger, N.



- 721 Caud, Y. Chen, L. Goldfarb, M.I. Gomis, M. Huang, K. Leitzell, E. Lonnoy, J.B.R.
722 Matthews, T.K. Maycock, T. Waterfield, O. Yelekçi, R. Yu, and B. Zhou (eds.)].
723 Cambridge University Press, Cambridge, United Kingdom and New York, NY, USA,
724 In press, doi:10.1017/9781009157896.
- 725 Johansson, M. M., Björkqvist, J.-V., Särkkä, J., Leijala, U., and Kahma, K. K. (2022)
726 Correlation of wind waves and sea level variations on the coast of the seasonally ice-
727 covered Gulf of Finland, *Nat. Hazards Earth Syst. Sci.*, 22, 813–829,
728 <https://doi.org/10.5194/nhess-22-813-2022>.
- 729 Kalnay, E., Kanamitsu, M., Kistler, R., Collins, W., Deaven, D., Gandin, L., ... Joseph,
730 D. (1996). The NCEP/NCAR 40-year reanalysis project. *Bulletin of the American*
731 *Meteorological Society*, 77(3), 437–471. [https://doi.org/10.1175/1520-](https://doi.org/10.1175/1520-0477(1996)077%3C0437:TNYRP%3E2.0.CO;2)
732 [0477\(1996\)077%3C0437:TNYRP%3E2.0.CO;2](https://doi.org/10.1175/1520-0477(1996)077%3C0437:TNYRP%3E2.0.CO;2)
- 733 Kaplan, A., Kushnir, Y., Cane, M.A., Blumenthal, M.B., 1997. Reduced space optimal analysis
734 for historical data sets: 136 years of Atlantic sea surface temperatures. *Journal of*
735 *Geophysical Research* 102, 27835–27860. <https://doi.org/10.1029/97JC01734>
- 736 Kaplan, A., Kushnir, Y., Cane, M.A., 2000. Reduced space optimal interpolation of
737 historical marine sea level pressure. *Journal of Climate* 13, 2987–3002. DOI:
738 [https://doi.org/10.1175/1520-0442\(2000\)013<2987:RSOIOH>2.0.CO;2](https://doi.org/10.1175/1520-0442(2000)013<2987:RSOIOH>2.0.CO;2)
- 739 Llovel, W., Becker M., Cazenave A., Jevrejeva S., Alkama R., Decharme, B., Douville H.,
740 Ablain M. and B. Beckley, (2011). Terrestrial waters and sea level variations on
741 interannual time scale. *Global and Planetary Change*, Vol. 75, Issues 1–2, Pg 76–82,
742 ISSN 0921-8181, <https://doi.org/10.1016/j.gloplacha.2010.10.008>.
743 (<https://www.sciencedirect.com/science/article/pii/S0921818110002328>)



- 744 McPhaden, M. J., Zebiak, S. E., & Glantz, M. H. (2006). ENSO as an integrating concept in
745 Earth science. *Science*, 314(5806), 1740–1745. [https://](https://doi.org/10.1126/science.1132588)
746 doi.org/10.1126/science.1132588.
- 747 Mu, Y., H and Y. and W. Feng (2018). Assessment of sea level variability derived by EOF
748 reconstruction. *Geophysical Journal International*, 214, 79–87.
749 [doi://10.1093/gji/ggy126](https://doi.org/10.1093/gji/ggy126)
- 750 Natarov, S. I., Merrifield M. A, Becker, J. M. and P. R. Thompson (2017). Regional influences
751 on reconstruction global mean sea level. <https://doi.org/10.1002/2016GL071523>.
- 752 Nerem, R.S., D. P. Chambers, C. Choe, and G. T. Mitchum (2010), Estimating mean sea level
753 change from the TOPEX and Jason altimeter missions, *Mar. Geod.*, 33, 435–446.
754 <https://doi.org/10.1080/01490419.2010.491031>
- 755 Permanent Service for Mean Sea Level (PSMSL), 2023, "Tide Gauge Data", Retrieved 21 Mar
756 2023 from <http://www.psmsl.org/data/obtaining>.
- 757 Peltier GIA data sets, drad250.1grid.ICE5Gv1.3_VM2_L90_2012.nc (Vertical Land Motion
758 (GPS or GNSS) prediction for Altimetry and
759 dsea250.1grid.ICE5Gv1.3_VM2_L90_2012.nc for the relative sea level (tide gauge)
760 prediction.
- 761 Peltier W.R (2004) Global Glacial Isostasy and the Surface of the Ice-Age Earth: The ICE-
762 5G(VM2) model and GRACE. *Ann. Rev. Earth. Planet. Sci.* 2004. 32,111-149.
- 763 Piecuch, C. G. (2023). River effects on sea-level rise in the Río de la Plata estuary during the
764 past century. *Ocean Science*, 19(1), 57–75. <https://doi.org/10.5194/os-19-57-2023>
- 765 Piecuch, C. G., Bittermann, K., Kemp, A. C., Ponte, R. M., Little, C. M., Engelhart, S. E., &
766 Lentz, S. J. (2018). River-discharge effects on UnitedStates Atlantic and gulf coast sea-
767 level changes. *Proceedings of the National Academy of Sciences of the United States*
768 *of America*, 115(30), 7729–7734. <https://doi.org/10.1073/pnas.1805428115>



- 769 Piecuch, C. G., Dangendorf, S., Ponte, R. M., & Marcos, M. (2016). Annual sea level changes
770 on the north American northeast coast: Influence of local winds and barotropic motions.
771 *Journal of Climate*, 29(13), 4801–4816. <https://doi.org/10.1175/JCLI-D-16-0048.1>
- 772 Ray, R.D. and B. C. Douglas (2011) Experiments in reconstructing twentieth-century sea
773 levels, *Progress in Oceanography*, Volume 91, Issue 4, Pages 496-515, ISSN 0079-
774 6611, <https://doi.org/10.1016/j.pocean.2011.07.021>.
- 775 Ropelewski, C.F. and Jones, P.D. (1987) An extension of the Tahiti-Darwin Southern
776 Oscillation Index. *Monthly Weather Review* **115**, 2161-2165. doi: 10.1175/1520-
777 0493(1987)115%3C2161:AEOTTS%3E2.0.CO;2
- 778 Royston, S.; Watson, C.S.; Legrésy, B.; King, M.A.; Church, J.A.; Bos, M.S. Sea-level trend
779 uncertainty with pacific climatic variability and temporally-correlated noise. *J.*
780 *Geophys. Res. Ocean.* 2018, 123, 1978–1993. <https://doi.org/10.1002/2017JC013655>.
- 781 Strassburg, M. W., B. D. Hamlington, R. R. Leben, and K.-Y. Kim (2014), A comparative
782 study of sea level reconstruction techniques using 20 years of satellite altimetry data, *J.*
783 *Geophys. Res. Oceans*, 119, 4068–4082, doi:10.1002/2014JC009893.
- 784 Sturges W. and B.C. Douglas (2011). Wind effects on estimates of sea level rise. *J. Geophysical*
785 *Research*, Vol. 116, C06008, doi:10.1029/2010JC006492
- 786 The Climate Change Initiative Coastal Sea Level Team (2020). Coastal sea level anomalies
787 and associated trends from Jason satellite altimetry over 2002–2018. *Sci. Data* 2020, 7,
788 357. <https://doi.org/10.1038/s41597-020-00694-w>.
- 789 White, N.J., Haigh, I.D., Church, J.A., Koen, T., Watson, C.S., Pritchard, T.R., Watson, P.J.,
790 Burgette, R.J., McInnes, K.L., You, Z.-J., Zhang, X. and P. Tregoning (2014).
791 Australian sea levels -Trends, regional variability and influencing factors. *Earth-*
792 *Science Reviews* Volume 136, Pages 155-174. ISSN 0012-8252,



793 <https://doi.org/10.1016/j.earscirev.2014.05.011>.

794 (<https://www.sciencedirect.com/science/article/pii/S0012825214000956>)

795 Widlansky, M.J., Long, X. & Schloesser, F. Increase in sea level variability with ocean
796 warming associated with the nonlinear thermal expansion of seawater. *Commun Earth*
797 *Environ* **1**, 9 (2020). <https://doi.org/10.1038/s43247-020-0008-8>

798 WCRP Global Sea Level Budget Group (2018). Global sea-level budget 1993–present. *Earth*
799 *Syst. Sci. Data*, Vol 10 (3), pg 1551-1590. DOI: 10.5194/essd-10-1551-2018.

800 Yang, F., Zhang, L., & M. Long (2022). Intensification of Pacific trade wind and related
801 changes in the relationship between sea surface temperature and sea level pressure.
802 *Geophysical Research Letters*, **49**, e2022GL098052.
803 <https://doi.org/10.1029/2022GL098052>

804 Zhang, X., and J. A. Church (2012), Sea level trends, interannual and decadal variability in the
805 Pacific Ocean, *Geophys. Res. Lett.*, **39**, L21701, doi:10.1029/2012GL053240.

806

807



808

809 ***Data statement***

810

811 All data are freely available from data providers that is explained in detail in the Data and

812 Methods section of the paper.